Multi-sensor airborne lidar requires intercalibration for consistent estimation of light attenuation and plant area density

Grégoire Vincent, Philippe Verley, Benjamin Brede, Guillaume Delaitre, Eliott Maurent, James Ball, Ilona Clocher, Nicolas Barbier

Multi-sensor airborne lidar requires intercalibration for consistent estimation of light attenuation and plant area density

Grégoire Vincent[a*], Philippe Verley[a], Benjamin Brede[b,c], Guillaume Delaitre[a,e], Eliott Maurent[a,f], James Ball[a,g], Ilona Clocher[a,d], Nicolas Barbier[a]

Abstract

Leaf area is a key structural characteristic of forest canopies because of the role of leaves in controlling many biological and physical processes occurring at the biosphere-atmosphere transition. High pulse density Airborne Laser Scanning (ALS) holds promise to provide spatially resolved and accurate estimates of plant area density (PAD) in forested landscapes, a key step in understanding forest functioning: phenology, carbon uptake, transpiration, radiative balance etc. Inconsistencies between different ALS sensors is a barrier to generating globally harmonised PAD estimates. The basic assumption on which PAD estimation is based is that light attenuation is proportional to vegetation area density. This study shows that the recorded extinction strongly depends on target detectability which is influenced by laser characteristics (power, sensitivity, wavelength). Three different airborne laser scanners were flown over a wet tropical forest at the Paracou research station in French Guiana. Different sensors, flight heights and transmitted power levels were compared. Light attenuation was retrieved with an open source ray-tracing code (http://amapvox.org). Direct comparison revealed marked differences (up-to 25% difference in profile-averaged light attenuation rate and 50% difference at particular heights) that could only be explained by differences in scanner characteristics. We show how bias which may occur under various acquisition conditions can generally be mitigated by a sensor intercalibration. Alignment of

light weight lidar attenuation profiles to ALS reference attenuation profiles is not always satisfactory and we discuss what are the likely sources of discrepancies. Neglecting the dependency of apparent light attenuation on scanner properties may lead to biases in estimated vegetation density commensurate to those affecting light attenuation estimates. Applying intercalibration procedures supports estimation of plant area density independent of acquisition characteristics.

Introduction

Gas exchange processes between vegetation and the atmosphere are mediated by leaf surface. For example, canopy temperature, energy balance, and photosynthetic rate are related to the amount of leaf area (Bonan 2015) which is therefore a key variable in dynamic vegetation models. Estimation of Leaf Area Index in evergreen forests has nonetheless remained a challenge and LAI is still poorly resolved over space and time. This limits our ability to effectively initialize/calibrate/validate or otherwise constrain vegetation models. Ground-based methods of LAI measurements have well known limitations (Bréda 2003). Litterfall collection cannot provide direct information without prior knowledge of the leaf lifespan which itself is highly variable within site across species and environmental conditions (Osada et al. 2001; Reich et al. 2004; Laurans et al. 2012). Indirect optical methods such as LAI2000 instrument or hemispherical photographs essentially measure directional gap probability which allows to derive “effective LAI” rather than actual LAI (Chen et al. 1997). Effective LAI is the expected LAI given the observed directional gap probability under the assumption that light is intercepted only by leaves (no wood contribution) and that foliage has a spatially random distribution (no clumping).

Extending the definition of Leaf Area Index proposed by (Chen and Black 1991), Plant Area Index (PAI) can be defined as half the total plant area (considering all vegetation components including branches and trunks) per unit horizontal ground surface area (Fang et al. 2019). Similarly, Plant Area Density (PAD) is then half the total plant area per unit volume of canopy. In the present study we are concerned with PAI and PAD only and will not address the problem of estimating the contribution of woody elements to PAI.

Deriving PAI from Airborne Laser Scanning is an attractive alternative compared to other means of estimation (Morsdorf et al. 2006; Hopkinson and Chasmer 2007; Solberg et al. 2009; Vincent et al. 2017; Almeida et al. 2019; Arnqvist et al. 2020). In contrast with direct ground measurements of PAI which typically have a limited spatial coverage (Olivas et al. 2013), ALS can produce consistent estimates over large areas capturing spatial variability of plant area density, leading to more accurate spatially integrated estimates. Mapping PAI at landscape scale opens-up new opportunities to study sources of variation of PAI, or to use such information as initial condition for dynamic vegetation models (Longo et al. 2020). A key advantage of lidar over passive optical methods is that it provides 3D-explicit information on light attenuation which allows to estimate PAD per small unit volumes rather than for the entire canopy, thereby reducing the clumping bias issue to the subunit volume scale (Vincent et al. 2017).

Direct estimate of LAI from passive optical remote sensing are based on the selective absorption of solar radiation by green leaves in red and infrared bands. They tend to saturate at high LAI values (Zheng and Moskal 2009). For instance the Normalized Difference Vegetation Index (NDVI) saturates around LAI = 3.5 (Shabanov et al. 2005). Retrieval algorithms based on look-up tables derived for typical canopy structures using stochastic radiative transfer equations are more sensitive than direct correlative approaches. However uncertainty at high LAI remains high due to the sensitivity of retrieval algorithm to the surface reflectance precision which is limited by frequent cloud and aerosol contamination in the tropics (Fang et al. 2019). ALS derived estimates of PAI may also saturate in tall dense vegetation. Dense vegetation may indeed favour high pulse fragmentation rate with multiple returns of lower intensity. A significant fraction of the returns may remain below the sensor's detection threshold, but this issue has received little attention so far.

The recent increase in the number of surveys of individual sites that have multi-temporal lidar data has however led to greater scrutiny of the consistency between acquisitions, notably in terms of sensor induced systematic difference in PAI estimate. Shao et al. (2019) for instance have built on the Sustainable Landscape Brazil data set and compared 4 sensors and 16 pairs of multitemporal measurements. Each pair consisted of two lidar surveys conducted in different years. That study showed that a statistical intercalibration between sensors using a single multiplicative factor significantly improved consistency in PAI estimates obtained with different sensors.

Extending the analysis of Shao et al. (2019), in the present study we compare light extinction profiles in a tropical forest canopy obtained with three different lidar sensors and under various settings (different flight heights, or different transmitted power). The objectives were to evaluate the level of sensitivity of light extinction profiles to acquisition conditions and also to identify the sources of bias in order to better take them into account in multiple site or multiple date vegetation surveys when identical acquisition settings are not granted.

The manuscript is organised as follows. The material and methods section briefly describes the general modelling assumptions, the ray tracing software used to process the lidar data (http://amapvox.org), the study site, the laser systems tested and the different flight plans operated. Then the analysis is conducted in two steps. The first step consists in analysing, for the different scanning scenarios, the level of completeness of retrieval of lidar backscattered energy and the variability in lidar returns intensity. The objective of this first part is to determine a robust estimate of the contribution of individual returns to the interception of an emitted laser pulse. The second part explores the differences in light extinction profiles (proportional to PAD profiles) for the different scanning scenarios. Those profiles are produced by using the return weighting scheme determined in the first step. Different light extinction profile inter-calibration procedures are tested. The discussion section examines both sets of results and further explores how an absolute calibration might be achieved.

Material & Methods

Theoretical background

PAD estimation from ALS data

Most methods proposed for estimating PAI from airborne lidar data build on the fundamental dependency between plant area density and light extinction rate. The theory describing light attenuation through canopies has a long history (e.g. (Miller 1967; Ross 1981)) and has served as the basis for describing lidar pulse extinction in forest canopies.

The Beer-Lambert law is commonly used to describe light extinction through a canopy layer.

$$\frac{I_l}{I_0} = exp(-\lambda\, l) \qquad \textit{Equation 1}$$

Where I_0 is the incoming light intensity, I_l is the remaining light intensity after travelling a distance l through the canopy and λ is the attenuation coefficient. This attenuation coefficient is proportional to the Plant Area Density ($m^2.m^{-3}$) and is also affected by other vegetation characteristics such as clumping and orientation of scatterers which may further introduce a dependency of attenuation on light incidence angle (Bréda 2003).

ALS derived canopy transmittance is obtained from the analysis of the return pulse waves of light reflected by the targets. Multiple hits occur if successive targets only partially intercept the source light pulse. If the targets are sufficiently large and sufficiently distant from each other, then distinct returns can be recorded. For each emitted pulse, some systems record all detectable returns (e.g. Riegl LMSQ 780, Riegl VUX-1UAV this study). Other systems are limited to a fixed maximum number of returns (e.g. five returns for the Riegl miniVUX, this study). Lidar systems typically record the strength of the backscattered echoes (often the peak power). However, a proper radiometric calibration is required to gain access to the echo energy (Wagner 2010).

In a detailed simulation study, Yin et al. (2020) examined the performance of various descriptors extracted from ALS data which had previously been used to estimate canopy transmittance and PAI. The metrics considered were derived from a ratio of traversing pulses over entering pulses. They differed however in the choice of the return numbers used for calculation (first, last, both, all) and whether these were weighted or not, and in the former case how they were weighted: by the inverse of the echo number per shot or by the recorded return intensity. They concluded that methods using return intensity for weighting the echoes were more accurate overall and less influenced by variations in footprint size, leaf area, vegetation cover, and foliar dimensions than the methods based on return counts only. Unfortunately, even when the individual echo energy is retrievable from the recorded signal, the physically based approach advocated by the authors may not be generally applicable. Indeed, the heterogeneity of a forest canopy and the high variability in optical properties of natural surfaces which affect the amount of light reflected towards the sensor may largely obscure the link between the target projected area and the returned energy (see below).

The lidar signal may also vary with atmospheric characteristics. If atmospheric conditions are known, the attenuation of lidar signal can be estimated from atmospheric transfer simulations (Wagner 2010). Alternatively, flight campaign calibration using targets of known optical properties can be attempted. Atmospheric extinction generally results both from scattering and absorption. Effect of atmospheric water content in the infra-red range was examined for laser ranger finders operating at 905 nm and 1550nm (Wojtanowski et al. 2014). That study reported a low impact of atmospheric humidity on extinction coefficients at both wavelengths. Fog however significantly decreased the detection range at both wavelengths and more so at 1550nm.

Surface wetness may also affect lidar return signal strength significantly. Kaasalainen et al. (2009) reported a decrease in reflectance of a series of targets (sand, brick, concrete) of 30-50% between dry and wet surfaces. WeiChen et al. (2015) operating a Leica ALS60 under different acquisition configurations reported a penetration rate (defined as the proportion of pulses generating a ground return to the total number of emitted laser pulses) reduced by approximately 25% in case of wet ground. This was attributed to the low reflectance of water in the near infrared range beyond 800 nm.

Lidar back-scattering model

For a target with Lambertian surface, larger than the foot print size and of solid angle π steradians the following relation between the received Power P_r to the transmitted power P_t has been proposed (Höfle and Pfeifer 2007)

$$P_r = \frac{P_t D_r^2 \rho}{4R^2} \eta_{sys} \eta_{atm} cos\alpha \qquad \textit{Equation 2}$$

Where R is the distance from sensor to target, α is the incidence angle, η_{sys} and η_{atm} are system and atmospheric transmission factors respectively, D_r is the receiver aperture diameter, and ρ is the target reflectance.

η_{sys}, D_r are considered constant for a given flight campaign and variation in η_{atm} between flight lines may be neglected in first approximation. Variation in η_{atm} is implicitly neglected between flight campaigns.

Critically, when using lidar one derives transmittance (or attenuation) from a measurement of reflected, not transmitted light. An implicit assumption is that all the hits will generate a return wave detectable by the sensor or, at least, that undetectable targets are sufficiently few to be ignored without significantly biasing transmittance estimation. However, this may not hold true at all times. Vegetation is typically composed of many scatterers, irregular in their spatial distribution, size, orientation and shape. Small or poorly reflective targets may not backscatter enough energy towards the sensor for a return to be detected. A fraction of the laser pulses may also be deflected away from sensor due to specular reflection as it is commonly observed over water bodies.

The energy associated with each return will depend on the fraction of the pulse which is intercepted as well as on the reflectivity and orientation of the intercepting surface (Höfle and Pfeifer 2007; Yin et al. 2020). Natural surfaces, however, tend to have highly variable optical properties (across material e.g. wood versus leaves, between ground and vegetation, depending on surface wetness, etc) which limits our ability to precisely characterise those properties.

Light attenuation profile computation

AMAPVox (http://AMAPVox.org) is an open source software designed to analyze lidar-vegetation interactions. It can process various discrete lidar data type: single or multiple returns, terrestrial or airborne.

AMAPvox tracks every laser pulse through a 3D grid (voxelized space) from the laser head to the last recorded hit. The effective sampling area of each laser pulse (or fraction of pulse in case of multiple hits) is computed from the theoretical beam section (a function of distance from laser and divergence of laser beam) and the remaining beam fraction entering a voxel. Different weighting options of individual returns are available which may include the individual return intensity. This information is combined with the optical path length of each pulse entering a voxel to compute the local attenuation per voxel. Different estimation procedures are provided in the AMAPVox software (Vincent et al. 2021). In the present study we used the maximum likelihood estimate of the attenuation coefficient coined “Potential Path Length” in AMAPvox (Vincent et al. 2021). This 3D description of local attenuation can then be horizontally integrated under consideration of the ground elevation to compute canopy attenuation profiles.

Study location

The lidar overflights were conducted over the experimental site of Paracou in French Guiana (see location map in (Vincent et al. 2012)) during the annual long dry season (September-November) in 2016, 2019 and 2020. The mean canopy height of the forest at Paracou is c. 27.8 m (standard deviation = 3.0) and the mean basal area c. 30m^2/ha in the unlogged plots (Vincent et al. 2010; Vincent et al. 2012). Two regions of interest were arbitrarily selected (a 1.4-ha plot and a 2-ha plot) that are covered with undisturbed old growth tropical moist forest (Figure 1).

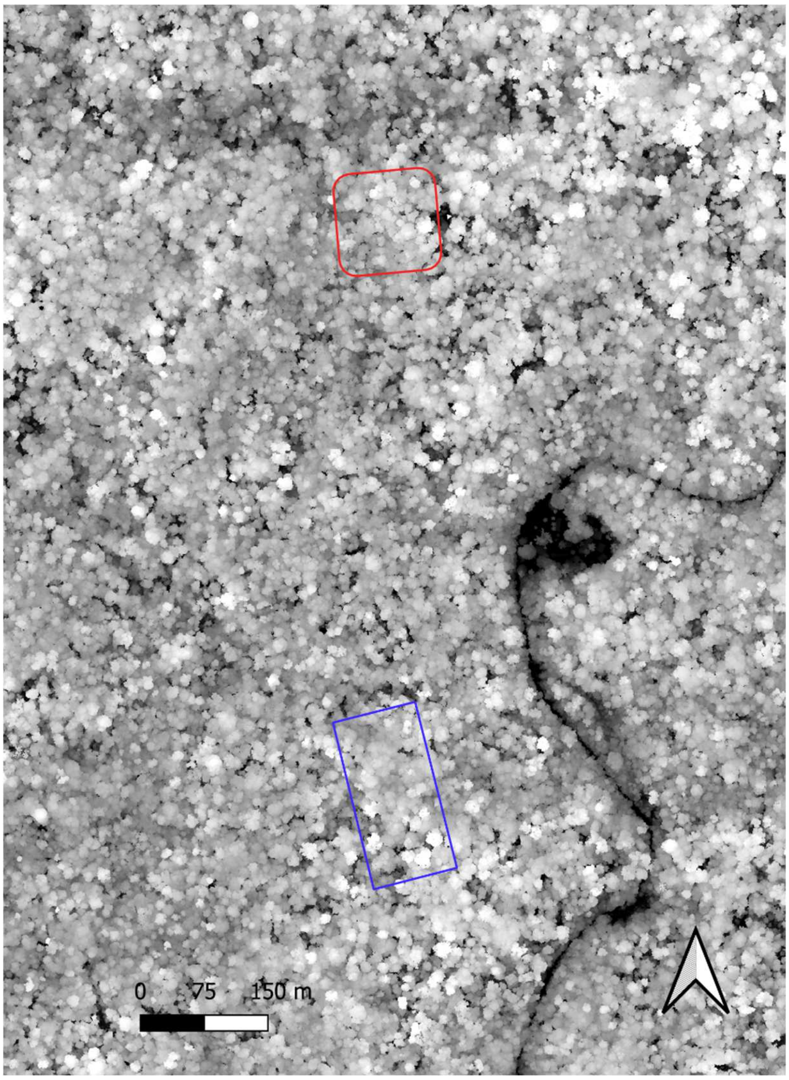

Figure 1: Paracou canopy height model (2019) with outline of ROI1 (red) and ROI2 (blue)

Lidar Systems

The *RIEGL* miniVUX-1UAV (905 nm) is a lightweight UAV-borne laser scanner, designed specifically for integration with UAV (Table 1). It uses online waveform processing, multi-target resolution (up-to 5 target echoes per laser shot). Beam divergence (measured at 50% peak intensity) is less than 1.6 x 0.5 mrad (RIEGL Laser Measurement Systems 2020). The long axis of the resulting elongated footprint is 16 cm and the short axis 5cm at 100m distance with a resulting footprint area of 0.008 m^2.

The RIEGL VUX-1UAV (1550nm) is about twice as powerful (Table 1) and heavy as the miniVUX. The Pulse Repetition Rate (PRR) of the VUX is adjustable from 50kHz to 550kHz. As the product of PRR and pulse power is constant changing PRR also affects pulse power (RIEGL Laser Measurement Systems 2020). The divergence is less than 0.5 mrad ($1/e^2$). The foot print diameter is 5 cm at 100m distance (0.002 m^2).

The RIEGL LMS-Q780 (1064 nm) is designed to be carried onboard a manned aircraft. It is a digital full waveform sensor that provides access to detailed target characteristics by digitizing the echo signal online during data acquisition and also allowing subsequent full waveform analysis. Beam divergence (measured at the $1/e^2$ point) is less than 0.25 mrad (RIEGL Laser Measurement Systems 2015). The footprint diameter is 22.5 cm at 900m distance (area of 0.04 m^2) and 11.25 cm at 450m (area of 0.01 m^2).

Beam divergence increases from 0.25 mrad (LMS-Q780) estimated at 0.135 peak power to 1.6*0.5 mrad (minivux) estimated at 50% of peak power. The footprint shape of the miniVUX is not circular and the divergence is given in two orthogonal directions. The difference in divergence is large and not easy to properly quantify given the different definition used for the miniVUX and the other two sensors. Importantly increased beam divergence means more rapid decrease in target irradiance (i.e. radiant flux received per unit area) which varies as the inverse of footprint area.

Table 1: Lidar sensor characteristics

Characteristic	LMSQ780	VUX-1UAV	miniVux -1 UAV	Comments
Weight	20 kg	3.65kg	1.6kg	-
Laser wavelength	1064 nm	1550 nm	905 nm	-
Beam divergence (mrad)	<=0.25	<=0.5	<=1.6*0.5	Different definition of divergence used for miniVux
Footprint diameter	22.5 cm @ 900m	5cm @ 100m	16*5 cm @ 100m	Non-spherical foot print of miniVUX
Pulse duration and range resolution	4.5 ns (0.75 m)	3 ns (0.45 m)	6 ns (0.9 m)	range resolution is defined as (group velocity * pulse duration) /2 (Wagner et al. 2006)
Adjustable power	Yes	Yes	No	
Maximum range (natural target of reflectivity > 60%)	2400m @25% power	660m @100% power	290m @100% Power	Assuming 23 km visibility, flat target in excess of foot print size, orthogonal to laser beam
Maximum number of recorded returns per pulse	Unlimited (observed 7)	Unlimited (observed 9)	5 (observed 5)	

We used the extra-byte information provided by RIEGL instruments (Riegl Laser Measurement Systems 2019) to normalize the return intensity with regard to distance as explained in the next paragraph.

All three instruments record the signal amplitude which is the optical input power relative to the instrument detection threshold (in dB).

For the miniVUX-1UAV and the VUX the normalized intensity was simply taken as the target relative reflectance value, i.e. the ratio of the actual echo amplitude to the amplitude of a white flat target at the same range, orientated orthonormal to the beam axis, and with a size in excess of the laser footprint. This was expressed as a fraction (between 0 and 1) rather than in dB, so that reflectance of successive echoes generated from a single emitted pulse could be meaningfully summed.

For the LMSQ780, normalized intensity was taken as (Vincent et al. 2017)

$$I = 10^{A/10} * d^2 * W * K \qquad \text{equation 3}$$

Where A (amplitude) is the optical power in dB, d (range) is the distance from source to target in m, W (pulse width) is defined as full width at half maximum of the received echo signal and is measured in nanoseconds (ns), and K is an arbitrary constant.

In the rest of the manuscript, intensity refers to the above-mentioned normalized intensities which are corrected for target range dependency. Note that while intensity values can be meaningfully compared for VUX and miniVUX data, the LMSQ780 values are provided on a different scale.

Flight plans

Two different tracts of undisturbed forest outlined on Figure 1 served to compare sensors, hereafter referred to as ROI1 (1.4ha) and ROI2 (2ha).

ROI1 flight plans

On this area we compared the LMSQ780 (different transmitted power and different flight heights) with the miniVUX-1UAV (operated at different flight heights). Scanning angles of all flights were limited to +/- 15 degrees off nadir to control for possible anisotropy in light extinction.

We considered two different campaigns operating the LMSQ780 over the same region of interest. Those campaigns took place in October 2016 and November 2019, both during the dry season. Due to variation in flight altitude and number of contributing flight lines (Table 2 and Table 3) the final pulse density varied across the different flight configurations from 9 to 22 pls. m^{-2}. Pulse density achieved with the miniVUX-1UAV (MNVX) was an order of magnitude higher, between 175 and 186 pls. m^{-2} (Table 3).

List of flights over ROI 1

- LMSQ780 (ALS) 19 September 2016, 3 flight heights (430m, 630m and 830m) and 2 transmitted power (6% and 12% full power)
- LMSQ780 (ALS) 15 November 2019, single flight height (900m), 25% full power
- MNVX (UAV-LS) 19-20 October 2020, 3 flight heights

ROI2 flight plans

Over the second ROI all data were acquired the same year during the dry season. Scanning angles of all flights were also limited to +/- 15 degrees off nadir.

List of flights over ROI 2

- LMSQ780 (ALS) 15 November 2019 single flight height, 25% full power, pulse density 19 pls.m^{-2}.

- MNVX (UAV-LS) 18 October 2019 single flight height, pulse density 85 $pls.m^{-2}$.
- VUX (UAV-LS) 10-21 October 2019 single flight height, 3 power levels (100%, 33%, 18%) and pulse densities (64, 187 and 369 $pls.m^{-2}$).

Lidar data processing and data analysis

The complete LMSQ780 2019 data set was used to produce a Digital Terrain Model. The consolidated pulse density was 40 $pls.m^{-2}$ for a scanning swath angle of +/- 30 degrees. Ground point filtering procedure is described in Appendix 1. All returns less than 50cm above the modelled ground surface were considered ground points to compute the three following indicators: ground point density ($pt.m^{-2}$), fraction of transmitted pulses reaching the ground (%), and proportion of energy reaching the ground. In the latter case, ground returns were weighted by the inverse of their return rank.

In the first part, we analyse the overall statistics per flight to firmly establish that target detection rate varies with at-canopy-irradiance (radiant power received per unit area of surface) for all three sensors.

Focusing on single (i.e. potentially unfragmented) returns we then investigate how reflectance varies across space. We illustrate the variability in reflectance across individual crowns by mapping single return intensity for the three sensors (ROI2). We further examine the dependency of single return intensity to canopy depth and height above the ground for the different sensors using multiple linear models. We also examine how individual return intensity varies with return rank. These pieces of information are combined to determine the individual return contribution to light interception used when computing light extinction with AMAPVox (part 2).

In the second part we move on to compare light extinction profiles for the different flights. The LMSQ780 2019 data were considered as the reference data when intercalibrating profiles as this campaign covered both ROIs.

Lidar data were voxelized at 2x2x2 m resolution. This resolution ensured that at least 90% of the lower most voxels were sampled by the reference lidar campaign (Appendix 2). A mean attenuation profile was computed for each flight over the areas of interest. Sensitivity of attenuation profiles to pulse density was found to be low. For instance, a 50% thinning of lidar pulses applied to the reference flight (density reduced to 10 emitted pulses per m^2, c. 20 return pulses) generated a relative Root Mean Square Error (RMSE) of less than 2% in the attenuation profile values. This was in line with previous observations reporting stable LAD profiles (at ¼ ha resolution) above 20 return pulses per m^2 (Shao et al. 2019).

The calibration procedure involved fitting the targeted attenuation profile to the reference profile. This was achieved by linear regression using R software (R Core Team. 2022) . Calibration functions were adjusted at the level of the vegetation profile rather than the individual voxel level. Indeed, given the uncertainty of individual voxel estimations (which acted as the predictors in the regression as well as the response variable) the regressions would have been biased (Frost and Thompson 2000). This uncertainty at voxel scale was systematically higher for lower vegetation layers due to the lower sampling intensity consecutive to the attenuation of the lidar signal travelling down the canopy. This uncertainty was further amplified by the time difference between some of the campaigns which were compared (e.g. LMSQ780-2019 vs MNVX-2020 or LMSQ780-2019 vs LMSQ780-2016).

Simple linear regressions without intercept were always considered first (corresponding to a single calibration coefficient). Additional predictors such as mean distance to laser or mean canopy depth (i.e. distance from top of canopy) were also tested to try to improve the fit.

Results

Global statistics per flight

During the ALS campaign conducted in 2016 various flight heights and laser power settings were compared. Reducing transmitted power (compare column 2 and 3, in Table 2) led to a decrease in mean number of returns per pulse, and a decrease in the cumulated fraction of pulses reaching the ground. Reducing flight height (compare column 1 to 2 in Table 2) led to an increase in mean return number per pulse, an increase in the proportion of pulses triggering a ground return and an increase in the cumulative fraction of pulses reaching the ground.

MiniVUX (Table 3) and VUX (Table 4) had lower penetration than LMSQ780 as measured by the lower fraction of pulses reaching the ground and the lower cumulated fraction of pulses reaching ground. MiniVUX and VUX also had fewer returns per pulse and fewer pulses generating more than one return. The miniVUX and VUX sensors showed trends in relation to change in canopy irradiance similar to the LMSQ780 both in terms of number of returns per pulse and penetration.

*Table 2: **ROI 1** (1.4 ha) statistics computed for 2016 ALS flights (2016) –*

LMSQ780 - flight height	High	Low	Low
Power setting	12%	12%	6%
Number of Flight lines	4	1	2
Median Height above ground in m + [min;max]	835 [802;849]	422 [421;425]	427 [424;436]
Average Foot print size at ground level (cm^2)	342	87	90
Reflectance detection threshold at ground level Beam orthogonal to target, no fragmentation, clear sky*	11%	<5%	5%
Mean scan angle from vertical (deg) + [min;max]	-2.14 [-7;+2]	-0.05 [-13;+13]	-3.83 [-13;+5]
Pulse density ($pls.m^{-2}$)	19	9	17
Ground point density ** ($pt.m^{-2}$)	0.89	0.70	0.97
Shots reaching ground **	4.8 %	7.6 %	5.7%
Cumulated fraction of returns reaching ground ***	1.6 %	2.1%	1.7%
Mean Number Of Returns per pulse	1.95	2.23	2.05
Fraction of Single Returns	0.36	0.29	0.34

* (RIEGL Laser Measurement Systems 2022)
** all returns up to 50cm above the modelled ground surface included
*** assuming balanced fragmentation

*Table 3: **ROI 1** (1.4 ha) statistics computed for DLS (2020) and LMSQ780 (2019) flights-*

	LMSQ780	MNVX Lowest height	MNVX Medium height	MNVX Highest
Flight code		195113	110932	201241
Power setting	25%	100%	100%	100%
Median Height above ground in m + [min;max]	891 [865;937]	58 [56;61]	71 [68;74]	104 [101;108]
Reflectance detection threshold at ground level Beam orthogonal to target, no fragmentation, clear sky*	7%	<5%	<5%	8%
Average Foot print size at ground level (cm^2)	360	27	40	87
Mean scan angle from vertical (degrees)	+0.36	+0.16	+0.05	-0.02
Pulse density **	22 (40)	160 (557)	175 (678)	173 (602)
Ground point density *** ($pt.m^{-2}$)	1.21	3.95	3.63	3.21
Shots reaching ground ***	5.4%	2.5%	2.1%	1.9%
Cumulated fraction of returns reaching ground ****	2.1 %	1.1%	1.0%	0.9%
Mean number of return per pulse	2.2	1.45	1.42	1.40
Fraction of single returns	0.28	0.64	0.66	0.66

* (RIEGL Laser Measurement Systems 2022)

**+/-15 degrees (full density in brackets)
*** all returns up to 50cm above the modelled ground surface included
**** assuming balanced fragmentation

*Table 4 : **ROI 2** (2 ha) statistics computed for 2019 ALS, MNVX and VUX flights-*

	LMSQ780	MNVX	VUX 100kHz	VUX 330kHz	VUX 550kHz
Power setting	25%	100%	100%	33%	18%
Median Height above ground in m + [min;max]	904 [878;927]	82 [78;85]	118 [105;129]	117 [105;127]	117 [106;127]
Reflectance detection threshold at ground level ; Beam orthogonal to target, no fragmentation, clear sky*	7%	<5%	<5%	5%	9%
Estimated Foot print size at ground level (cm2)	401	54	27	27	27
Mean scan angle	1.08	1.24	0.59	0.62	0.65
Pulse density **	19 (34)	82 (218)	65 (141)	187 (408)	369 (792)
Ground point density*** (pt.m^{-2})	0.97	0.71	2.58	5.70	8.82
Shots reaching ground***	5.2%	0.9%	4.0%	3.0%	2.4%
Cumulated fraction of pulses reaching ground****	2.0 %	0.4%	1.4%	1.2%	1.1%
Mean number of returns per pulse	2.2	1.4	1.8	1.7	1.6
Fraction of single returns	0.29	0.66	0.47	0.49	0.53

* (RIEGL Laser Measurement Systems 2022)
**+/-15 degrees scan angle (full density in brackets)
***all returns up to 50cm above the modelled ground surface included
**** assuming balanced fragmentation

Variability in backscattered energy

Single returns intensity varies across crowns

We selected single returns classified as vegetation in 3 sample datasets over ROI2 (LMSQ780 25% power, VUX full power, miniVUX) to map the canopy reflectance (Figure 2). Single return intensity was clearly structured per crown. It was also noticeable that ranking of individual crown reflectance was not consistent across sensors.

On Figure 2- right panel the high intensity returns which appear in yellow can distinctively be traced to branches and trunks by examining the point cloud. Wood reflectivity is indeed typically higher than leaf reflectivity at 1550 nm (Brede et al. 2022).

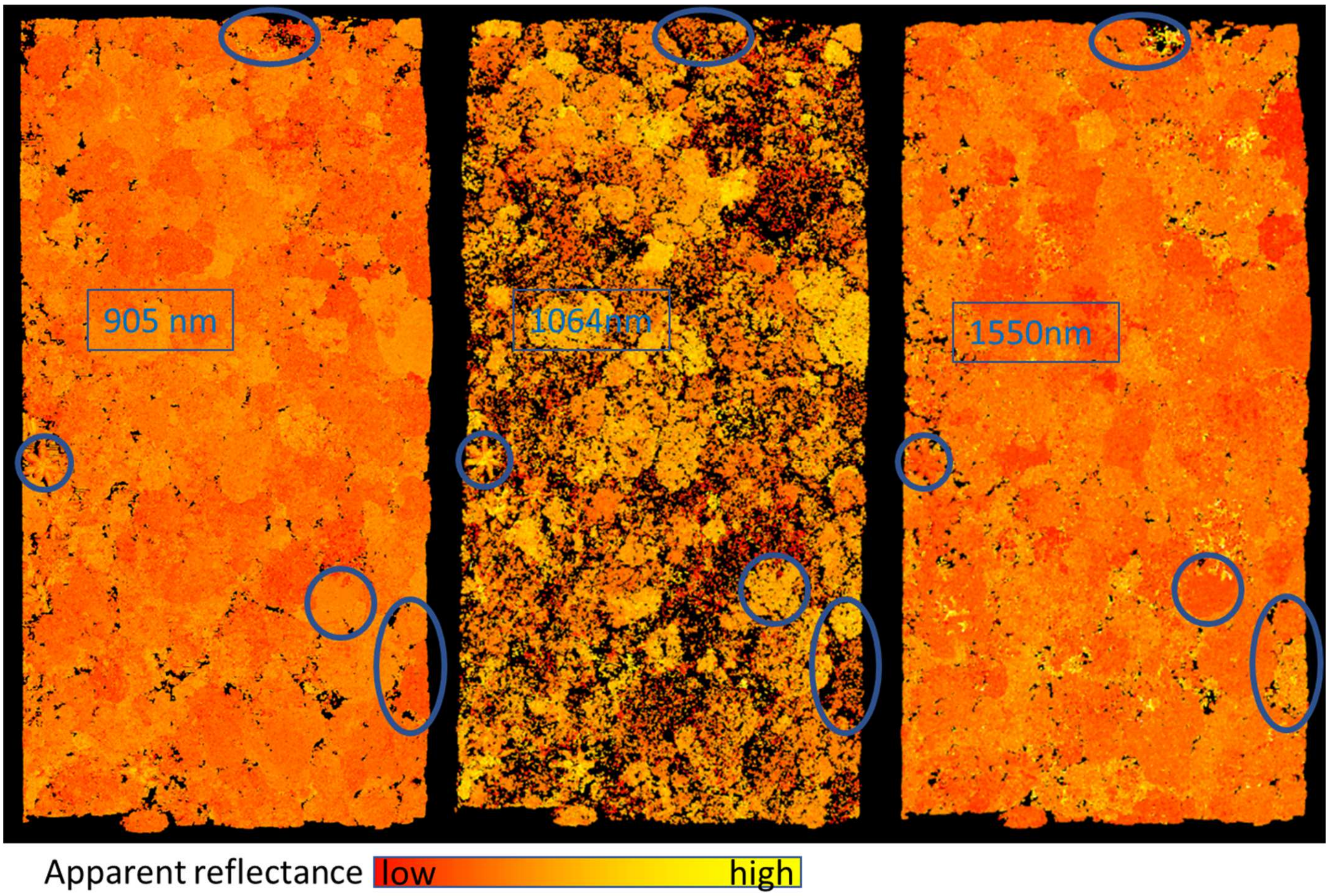

Figure 2: Intensity of single returns (ROI 2) by three sensors of different wavelength illustrating crown to crown variation. Left miniVUX 905nm, center ALS 1064nm, right VUX (scan angle restricted to +/-15 degrees) - Different absolute scales are used for different sensors; Some crowns are highlighted to illustrate the fact that intensity ranking is not preserved across laser wavelengths

Single return intensity varies with canopy depth

We examined whether a systematic change in reflectivity along the vertical canopy profile would occur as a consequence of a change in vegetation characteristics (leaf/wood ratio or leaf water content for instance). Because position in canopy and return rank were highly correlated due to the overhanging scanning position, we restricted the analysis to single returns for all flights, excluding ground points. We normalized individual return intensity by dividing by the mean return intensity for each flight. We then fitted a linear model with a fixed intercept equal to one (the overall mean intensity), with height above ground (HAG) and distance from top of canopy (DTC) as continuous predictors (no interaction term). Albeit both predictors were correlated (typically r~0.75) dropping one of the predictors often significantly reduced the goodness of fit (Table 5).

While the proportion of total variance in single return intensity attributable to position in canopy (HAG + DTC) was always low to very low (Table 5) it was also statistically highly significant. When considered individually, DTC usually made a larger contribution than HAG to r^2 (Table 5, last two columns). Recorded intensity by the VUX (1550nm) showed the largest variation with canopy depth.

Table 5 : R^2 of linear prediction model of single return intensity as a function of HAG, DTC or both (Full); HAG: Height Above Ground, DTC: Distance to Top of Canopy; All models have F statistic with p value < 0.001). The coefficients of both predictors for the full model are also reported (HAG eff. And DTC eff.)

ROI	Sensor	Flight	Full model	HAG eff.	DTC eff.	HAG	DTC
1	miniVUX	58m AGL	0.024	-7.5E-03	-1.1E-03	0.004	0.011
1	miniVUX	71m AGL	0.003	-1.7E-03	-4.2E-04	0.001	0.000
1	miniVUX	104m AGL	0.021	-5.8E-03	-7.8E-04	0.002	0.011
1	LMSQ780	430m AGL 12% power	0.010	7.7E-03	2.3E-04	0.000	0.010
1	LMSQ780	430m AGL 6% power	0.002	2.8E-03	3.5E-05	0.000	0.002
1	LMSQ780	830m AGL 12% power	0.006	5.5E-03	5.1E-05	0.000	0.006
1	LMSQ780	900m AGL 25% power	0.001	-5.9E-04	-2.7E-04	0.001	0.000

2	VUX	100kHz-100% power	0.025	-1.0E-02	-1.1E-03	0.002	0.017
2	VUX	330kHz-33% power	0.041	-1.2E-02	-1.3E-03	0.002	0.028
2	VUX	550kHz-18% power	0.044	-1.1E-02	-1.3E-03	0.002	0.030
2	LMSQ780	900m AGL, 25% power	0.002	3.5E-03	1.3E-04	0.000	0.002
2	miniVUX	82m AGL	0.002	-1.7E-03	-3.2E-04	0.001	0.001

For each flight we then corrected the complete data for HAG and DTC estimated effects by applying the same multiplicative correction factor (function of HAG and DTC) which was estimated for single returns, to the entire set of vegetation returns. On this corrected data set we analyzed how the cumulated intensity per emitted pulse would vary with the number of returns per pulse. We also conducted this analysis on the uncorrected data set for comparative purposes (Figure 3). As a result of this correction, the initially observed trend for the VUX of mean cumulative return intensity to increase with pulse fragmentation almost disappeared (Figure 3F). This correction affected less the energy conservation patterns of the other sensors. It increased slightly the apparent loss with fragmentation observed for the miniVUX.

The mean cumulated intensity per shot varied with the level of pulse fragmentation (Figure 3). A decrease in mean return energy was noticeable from single to multiple return shots for LMSQ780 and miniVUX (both plots). This decrease in cumulated intensity was more pronounced for lower flight heights (at a given laser power) or for higher laser power (at a given flight height) see Figure 3A.

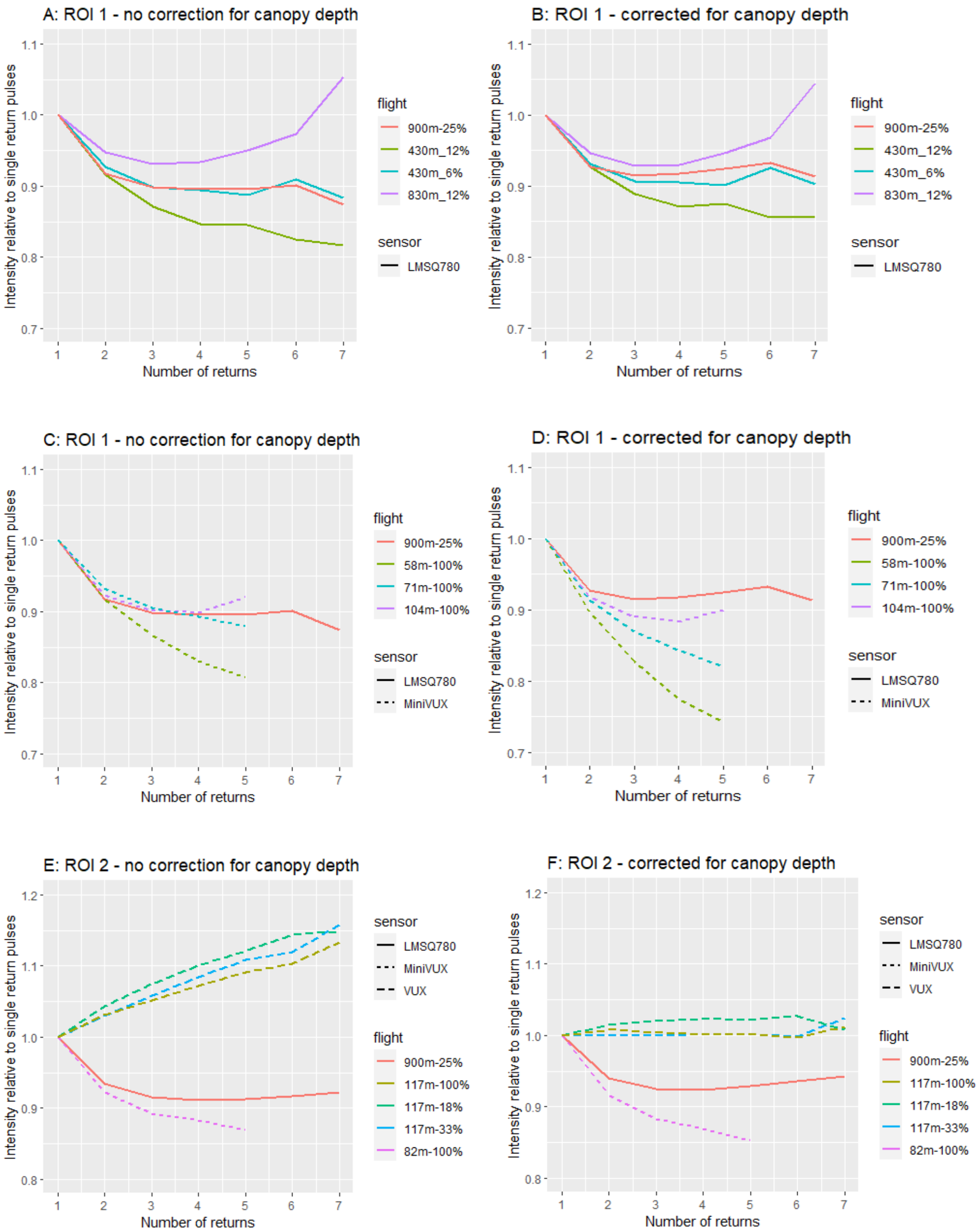

Figure 3 Mean cumulative intensity per shot (intensity) as a function of the number of detected returns (Number of returns); only shots not triggering a ground echo are considered. First line (A &B) considers different scanning settings for the same sensor. Second line (C & D) shows response for two different sensors. Third line (E & F) compares three different sensors. A, C & E (left): no intensity correction for canopy depth. B, D & F (right): systematic change in intensity occurring with canopy depth was corrected prior to analysis (see text).

The uncorrected VUX data showed an increase in cumulated intensity with degree of fragmentation (Figure 3E). After correcting for systematic variation of intensity with canopy depth this trend was barely discernible (Figure 3F). The strong dependence of return intensity on canopy depth, which was probably not completely compensated for, make this data set difficult to interpret in terms of patterns of backscattered energy retrieval. However, it can be noted that increasing the VUX power from 18% to 100% increased the mean vegetation single return intensity by 17% (from 0.24 to 0.29, Table 6), indicating that a fraction of the single returns were incomplete returns, at least when power was less than 100%.

Somewhat unexpectedly, decreasing the miniVUX flight height (and thereby increasing irradiance and detection rate) did not lead to a systematic increase in mean vegetation single return intensity (instead a less than 4% and non-monotonous change was observed across flights; intensity of single returns was 0.33, 0.32 and 0.34 for 58 m, 71 m and 104 m height of flights, ROI1-CNES). However, the decrease in cumulated return intensity with fragmentation was more pronounced at higher at-canopy irradiance (Figure 3C and 3D, dotted lines). This is consistent with an increased proportion of “incomplete returns” and a lower detection rate (lower number of returns) with decreased irradiance (Table 3) for higher flights.

In the case of the LSMQ780, it was observed that, like for the miniVUX (ROI1), higher at-canopy-irradiance was associated with a stronger decrease in cumulated intensity following fragmentation (compare for instance 900m_25% and 830m_12% or 430m_12% and 430m_6%, in Figure 3A or 2B). It was also found, like for the VUX (ROI2), that higher irradiance determined a higher mean vegetation single return intensity. For instance, single return intensity at 12% power was 649 and 702 (arbitrary units) for 830 and 430m flight height, i.e. an 8% increase followed from at-canopy-irradiance being multiplied by 4 (as footprint area was divided by 4).

The cumulated retrieved energy per shot appeared to plateau (or even to increase, see for ex. 830m_12% flight in Figure 3A or 3B) as the number of returns increased for the lowest at-canopy-irradiance values.

In addition, the mean vegetation to ground intensity ratio varied with wavelength as reported for ROI2 in Table 6. Values higher than one indicate a higher reflectivity of ground which may negatively bias the estimation of light extinction by vegetation. Indeed, if the compact background is more reflective than the porous medium in the foreground then it will be detected more effectively than potential targets in the foreground and transmittance may be overestimated. Conversely values lower than one may positively bias estimates of attenuation by vegetation. Those effects will affect detection rate more significantly under lower irradiance.

Mean single return ground intensity was larger than mean vegetation single return intensity for the VUX, and the ratio increased with at-canopy-radiance. So did the mean single return intensity as more partial hits were detected.

Table 6: Mean intensity of ground and vegetation single returns (ROI 2); standard deviation given in parenthesis

Sensor	Flight spec.	Ground	Vegetation	Ratio
VUX	100kHz - 100% power	0.415 (0.155)	0.286 (0.092)	1.45
VUX	330kHz - 33% power	0.375 (0.127)	0.262 (0.078)	1.43
VUX	550kHz - 18% power	0.320 (0.095)	0.239 (0.068)	1.34
LMSQ780	25% power – 900m AGL	211 (119)	209 (62)	1.01
miniVUX	82m AGL	0.303 (0.085)	0.334 (0.077)	0.90

We computed the intensity per rank (per number of return) for all flights over each ROI (*Table 7*) excluding all shots reaching the ground. The common general pattern was for intensity per return pulse to decrease with successive hits as the pulse effective footprint size (i.e. remaining foot print size after partial interception) was gradually reduced. As the number of returns increases above 4 or 5, a conditional sampling effect tended to compensate for this, since likelihood of detecting more targets is reduced if foremost targets are larger.

The weighting of individual return which was finally used for computing the attenuation profiles (next section) is depicted in Table 7 below. It was derived from data collected using LMSQ780 at 25% power over ROI 2. Note that for number of returns larger than 7 data from VUX at 100% power were used instead since no pulses with more than 7 returns were recorded using the LMSQ780 (Table 1).

Table 7: Mean relative intensity per return (corrected for systematic variation with canopy depth and height above ground)- ROI2 LMSQ780-25% complemented with VUX 100kHz for number of returns >7; relative standard error (%) of mean intensity in parenthesis. Excluding all shots reaching the ground.

Return rank Number of returns	**1**	**2**	**3**	**4**	**5**	**6**	**7**	**8**	**9**
1	1.00 (0.04)	-	-	-	-	-	-	-	-
2	0.66 (0.06)	0.34 (0.10)	-	-	-	-	-	-	-
3	0.45 (0.09)	0.35 (0.10)	0.20 (0.13)	-	-	-	-	-	-
4	0.33 (0.17)	0.30 (0.16)	0.22 (0.18)	0.15 (0.20)	-	-	-	-	-
5	0.25 (0.37)	0.24 (0.35)	0.21 (0.36)	0.17 (0.38)	0.13 (0.39)	-	-	-	-
6	0.19 (1.01)	0.21 (0.94)	0.18 (0.94)	0.17 (0.98)	0.14 (0.97)	0.11 (0.98)	-	-	-
7	0.15 (3.29)	0.17 (2.94)	0.16 (3.17)	0.16 (3.28)	0.14 (3.38)	0.12 (3.30)	0.10 (3.18)	-	-
8	0.11 (13.20)	0.19 (10.18)	0.23 (12.71)	0.08 (18.80)	0.09 (15.12)	0.15 (12.47)	0.08 (12.75)	0.07 (15.22)	-
9	0.28 (10.86)	0.18 (70.55)	0.05 (40.13)	0.05 (57.98)	0.22 (87.69)	0.14 (10.79)	0.03 (71.11)	0.02 (96.60)	0.03 (3.01)

By considering a single matrix of weights for all flights we assumed those weights to be valid across scanning scenarios. The actual pattern of pulse fragmentation is not expected to depend on the wavelength or the transmitted power. However, differences in detection rate across scanning scenarios will inevitably affect the relative intensity per return and therefore the mean weight per return. The matrix used is therefore necessarily approximate.

We also considered the option consisting in adjusting a matrix of weights derived from each flight data (with or without prior correction of intensity variation with canopy depth). Doing so did not systematically or significantly reduce discrepancy between raw profiles or corrected profiles (i.e. profiles obtained after applying a calibration function, see next section).

Concurrently to the decrease in return intensity with increasing return rank (Table 7), we observed (Figure 3 A, B, C, D) that higher fragmentation (higher number of returns per emitted pulse) was associated with a lower cumulative intensity.

Intercalibration of ALS flights

Can ALS flights be intercalibrated in such a way that overflights conducted under different acquisition settings at different dates or at different sites may still be compared meaningfully in terms of PAD? Attenuation profiles were adjusted to a reference profile derived for each ROI from the LMSQ780-2019 flight which covered both ROIs (Figure 1). Adjustment consisted in minimizing the squared distance between profiles. Two different models were used to fit the targeted profiles to the reference profile. The first one consisted in finding a single calibration coefficient, by fitting a linear regression without intercept between profile values. The second model included an intercept and an additional covariate, the mean distance to sensor of each vegetation layer. Note that this covariate was highly correlated with height above ground at plot scale (r>0.99).

Model 1

$$target_i = reference_i.\alpha + \varepsilon_i \qquad \text{equation 4}$$

Model 2

$$target_i = reference_i.\alpha + distance_i.\beta + \gamma + \varepsilon_i \quad \text{equation 5}$$

Where

i is an index referring to height (varies from 1 to 45 m above ground)

$target_i$ is the observed attenuation value at height i of profile to be adjusted

$reference_i$ is the reference profile attenuation value at height i distance$_i$ is the mean distance to laser of profile to be adjusted at height i

ε_i the error term to be minimized

A more complex model including mean canopy depth per layer as an additional predictor was also tested but did not improve the fit significantly.

ROI1. ALS extinction profiles (variable flight height and variable transmitted power) are presented in Figure 4. MiniVUX (multiple flight heights) extinction profiles are presented in Figure 5. Corresponding adjustment statistics are reported in Table 8.

ROI2. VUX (various transmitted power) and miniVUX (single flight) are presented in Figure 6. Corresponding adjustment statistics are reported in Table 9.

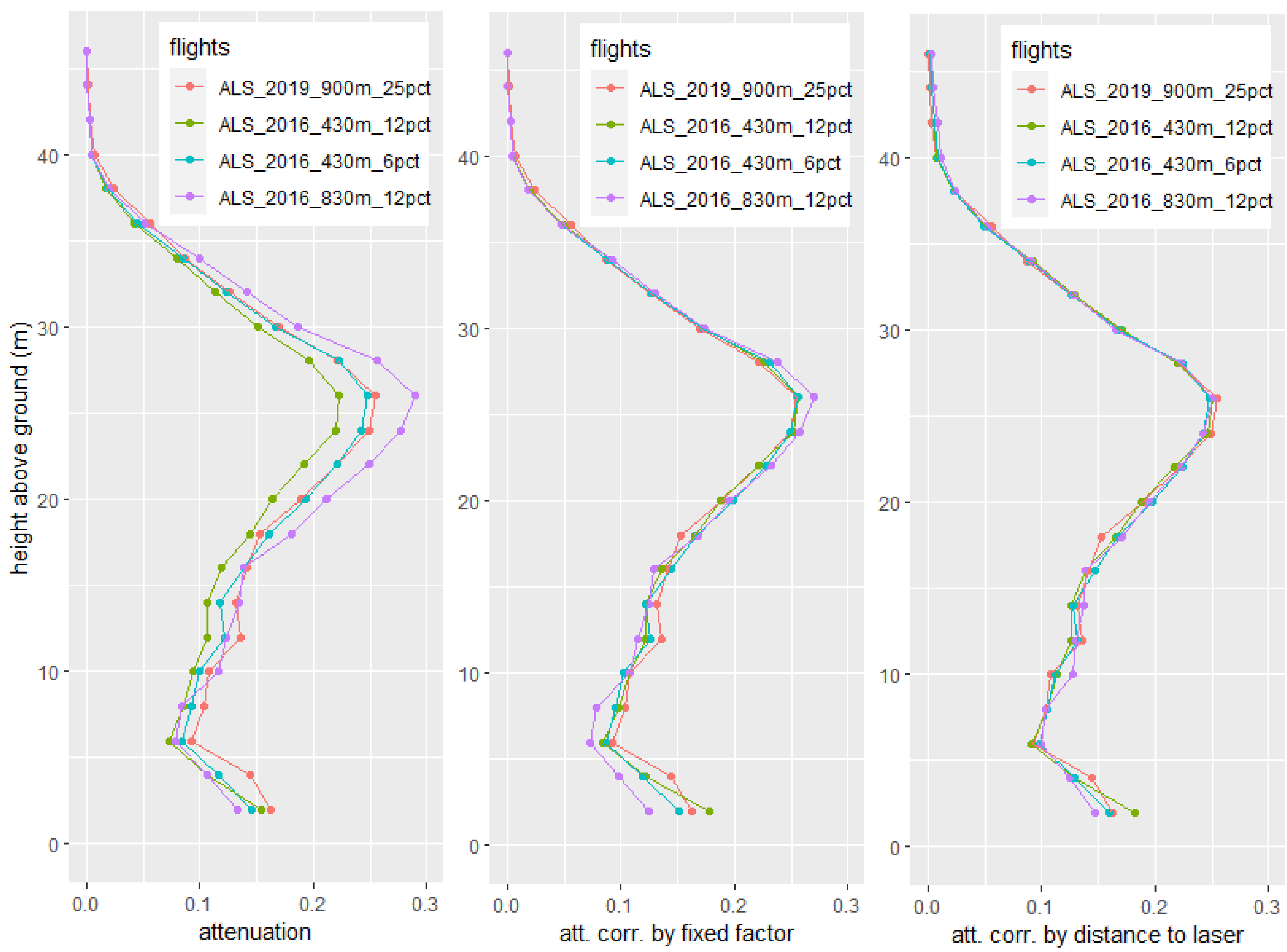

Figure 4: Inter calibration of ALS attenuation profiles obtained for different nominal flight heights (430m, 630m, 830m and 900m) and transmitted power (6%, 12% or 25% of full power). Left panel : raw profiles; center panel : profiles are adjusted to reference flight (900m 25%) by a simple constant correction coefficient; right panel : adjustment includes a linear effect of distance to laser.

Table 8: Attenuation profile adjustment statistics (ROI 1) - In bold lowest AIC and lowest residual standard error (rse) are highlighted showing improvement in fit when distance to laser is added as a predictor.

flight	rmse	rse_simple	calib. coef	rse_dist	AIC_simple	AIC_dist
ALS_430m_12pct	0.019	0.008	1.16	**0.008**	-203	**-203**
ALS_430m_6pct	0.009	0.007	1.05	**0.005**	-210	**-224**
ALS_830m_12pct	0.014	0.013	0.95	**0.008**	-172	**-197**
mnvx_low	0.019	0.011	0.89	**0.007**	-180	**-205**
mnvx_medium	0.028	0.011	0.83	**0.008**	-179	**-200**
mnvx_high	0.044	0.009	0.74	**0.009**	**-197**	-194

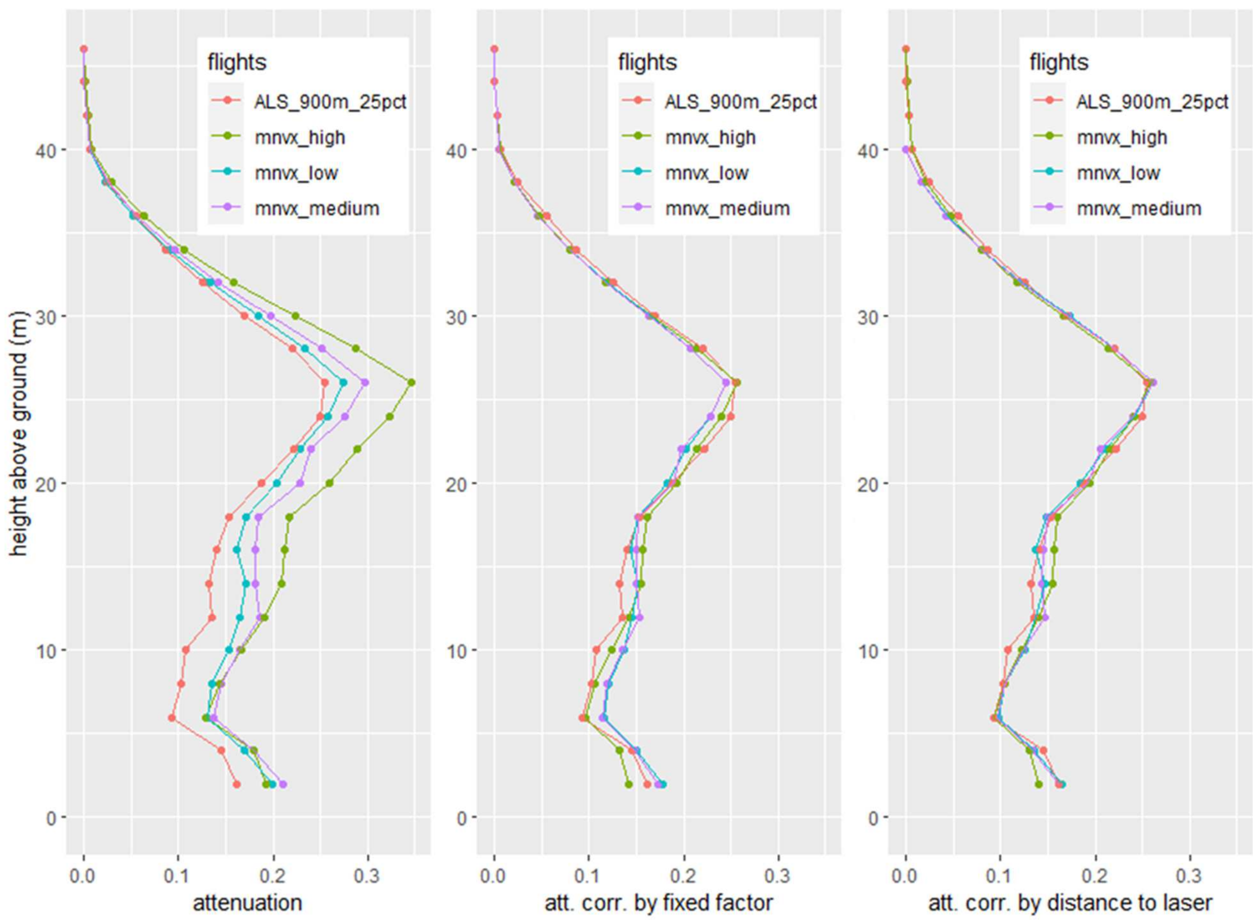

Figure 5: MiniVUX attenuation profiles obtained for different median flight heights above ground level (low = 58m, medium = 71m and high = 104m) plotted along ALS reference flight profile. Left panel: raw profiles; center panel: profiles are adjusted by means of a simple calibration coefficient ; right panel: calibration includes a linear effect of distance to laser.

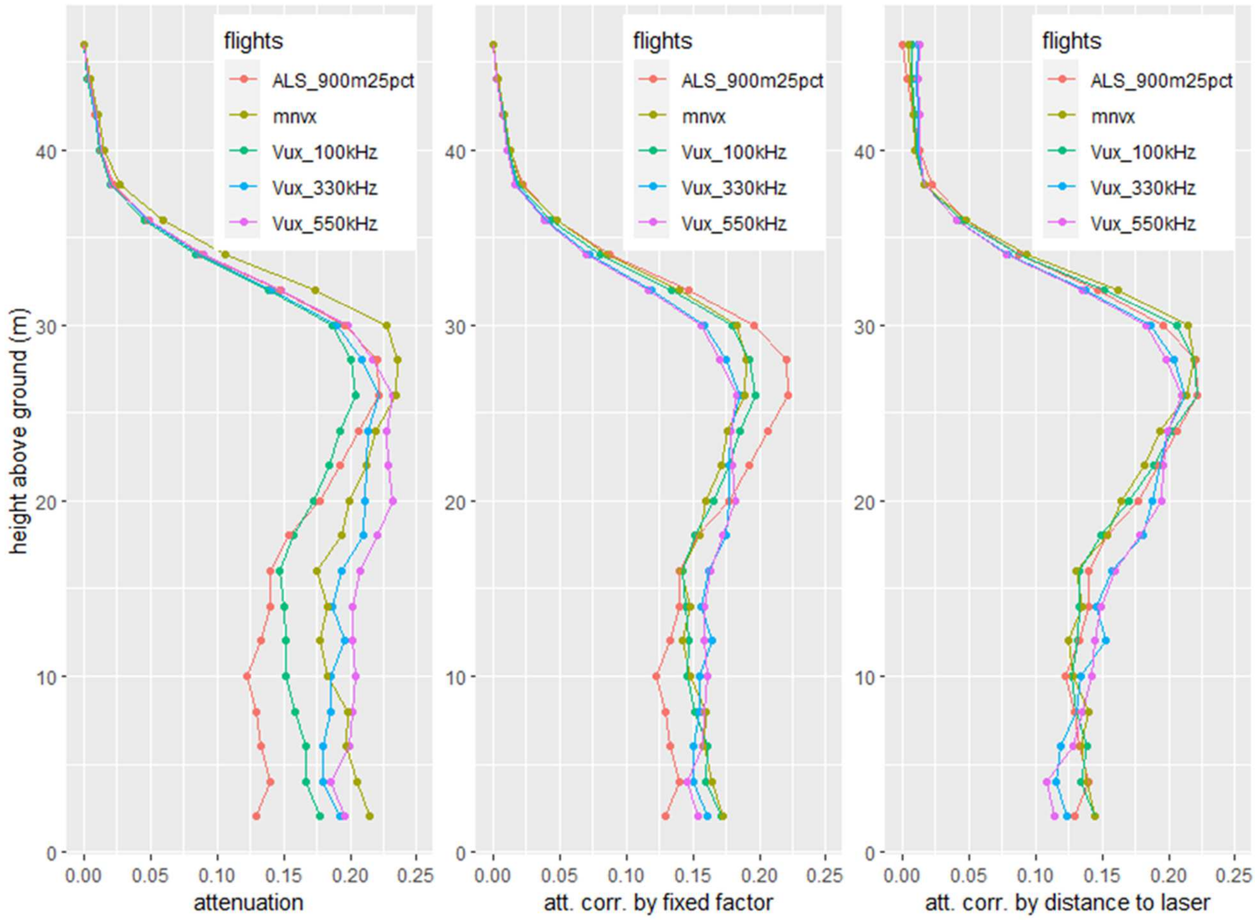

Figure 6: VUX attenuation profiles obtained for different power settings, with miniVUX profile and with ALS reference profile. Left panel: raw profiles; center panel:profiles are adjusted by means of a simple calibration coefficient ; right panel: fitting incorporates a linear effect of distance to laser

Table 9: Attenuation profile adjustment statistics (ROI 2) of UAV lidar flights against reference ALS profile - In bold lowest AIC and lowest rse are highlighted showing improvement in fit when distance to laser is added as model predictor.

drone	rmse	rse_simple	Calib.coef	rse_dist	AIC_simple	AIC_dist
MiniVux	0.039	0.020	0.81	**0.009**	-112	**-145**
Vux_100kHz	0.018	0.018	0.96	**0.006**	-117	**-163**
Vux_330kHz	0.035	0.024	0.84	**0.013**	-104	**-129**
Vux_550kHz	0.044	0.025	0.79	**0.015**	-102	**-123**

Divergence between 2016-ALS profiles and reference 2019-ALS profile were globally smaller than the divergence between UAV and 2019-ALS (Table 5 and Table 6). Lower at-canopy-irradiance flights had profiles showing higher attenuation (e.g. ALS_830m_12%, Figure 4-left panel), higher at-canopy-irradiance showed lower attenuation (e.g. ALS_430m_12%, Figure 4-left panel).

Divergence between UAV profiles and reference ALS profile increased with height of flight (miniVUX Table 5) and with lower laser power (VUX Table 6).

The model including distance-to-laser as a covariate usually improved the fit (lower rse) compared to the use of a simple calibration coefficient. The improvement was often very significant with a much lower AIC (Table 5 and Table 6). Improvement in consistency between profiles is illustrated in Figure 4, Figure 5 and Figure 6.

Residual error of VUX low power profiles (300kz and 500kHz Pulse Repetition Rates) was larger than in any other situation (see misfit in Figure 6 right panel).

Discussion

A general pattern was observed by which increasing at-canopy-irradiance led to higher penetration and higher fragmentation rate. This was in line with previous studies which have reported similar observations for other lidar sensors. Lee and Wang (2013) reported higher penetration rate (proportion of ground point) at lower flying altitude over a subtropical forest, both with Optech HD400 and Riegl LMS-Q680i. Næsset (2009) compared an Optech ALTM 1233 and an Optech ALTM 3100 operated at different flight heights and pulse repetition rates (PRR) over mature conifer forest. That study reported a decrease in the proportion of multiple echoes with increasing flying altitude and PRR. Such observations were made as part of a study exploring scanning settings impact on digital terrain model quality (Lee and Wang 2013) or a study exploring scanning settings impact on forest canopy metrics (Næsset 2009). They have not been interpreted in the context of Plant Area Density estimation from lidar data and the implication of such observations in terms of target under-detection do not seem to have not been fully recognized.

Part 1: individual return intensity analysis

This first analysis showed that apparent reflectance of vegetation targets was highly variable across tree crowns (Figure 1) and that it also varied with canopy depth (Table 5). Both observations were true for the 3 sensors tested but responses varied according to sensor wavelength. While reflectance is expected to vary with incident angle (see Equation 2 above), it is unlikely that spatial variation in leaf orientation might have been the main driver of the observed patterns of change in apparent reflectance since the response varied across sensors both in intensity and direction. The dependence of apparent reflectance on light incident angle could be further investigated taking advantage of the large field of view of the miniVUX and VUX sensors which were restricted to near-nadir incident angle in the present study (see Material and Methods section). Dependence on canopy depth was particularly strong for the VUX operating at 1550nm. We also found that a more complete retrieval of backscattered energy was achieved in case of higher at-canopy-irradiance and in case of lower fragmentation rate.

Cumulative backscattered energy typically declined with increasing fragmentation (higher number of returns per pulse). This may be a direct consequence of the intensity detection threshold as more fragmented pulses are more likely to generate undetected returns. This may also indicate that a higher pulse fragmentation decreases the detection rate. Successive hits by a downward travelling pulse do not only gradually reduce its footprint but also its compactness (Figure S1). As a consequence, detectability of small targets (relative to foot print size) will decrease and the proportion of undetected interceptions (backscattered energy below the detection threshold) will increase. This effect is expected to be dependent on the specific arrangement (size, density) of scatterers and its contribution is difficult to evaluate and likely to vary across vegetation types. Note that pulse compactness does not affect detectability of ground (non-porous target larger than foot print size) which will depend on ground reflectivity and remaining transmitted power. In some cases, we noted that higher fragmentation was associated with higher cumulative backscattered energy (see for ex. 830m_12% flight in Figure 3A or 2B). The underlying logic for what may appear as a paradox is in fact quite simple. The probability of detecting a target increases with target's reflectivity. Therefore, a high number of returns is more likely to be observed if targets are more reflective than average which also increases the cumulated energy per pulse. This pattern is expected to be weaker or even absent under high at-canopy-irradiance since more complete detection is less dependent on target reflectivity.

An increase in the at-canopy-irradiance was associated with a stronger drop in cumulative backscattered energy of multiple returns shots (fig 3). Such a pattern may be explained as follows . Pulses generating a single return may have been fully intercepted by a target larger than foot print size or, alternatively, may correspond to an incompletely obstructed pulse (a "partial hit") which let too little energy through (or a too highly fragmented pulse, see figure S1) for a second return to be triggered further along the optical path. This might occur frequently given the porous structure of the canopy. A typical echo is likely to be generated by interception of multiple scattered elements of foliage which might allow some light to continue travelling undetected down the optical path. Increasing the irradiance will increase the detection rate of secondary targets and thereby reduce the frequency of single returns corresponding to only partially intercepted pulses by a single target. As a result, the mean intensity of single returns (relative to the mean cumulated intensity of multiple returns) increases when at-canopy-irradiance increases.

We have no clear explanation for the fact mean single return intensity did not increase with increased at-canopy-irradiance for the miniVUX. This may be may be related to the change in size or shape of the footprint with distance. A lower flight height determines a smaller pulse footprint at the top of the canopy and hence a deeper penetration of pulse prior to triggering a return. The mean single return height was only slightly affected: respectively equal to 27.56, 27.40 and 27.26m for the 3 flight heights. This will nonetheless have affected mean irradiance of target and target reflectivity. A General Additive Model of intensity as a function of canopy depth (not presented) showed a non-linear trend of single return intensity with canopy depth in the upper canopy which might have compensated the expected increase in intensity.

High variability in target reflectivity made individual return intensity an unreliable proxy of the fraction of pulse intercepted per hit. Instead, we estimated the contribution of each return by the mean return intensity per return rank per return number (after excluding any shot reaching the ground).

In a previous study (Vincent et al. 2017) conducted with a different sensor (Riegl LMSQ560, 1550nm), the mean cumulative returned intensity per emitted pulse was reported to be independent of the number of returns per pulse. This was taken as an argument that undetected backscattered energy would either be small or independent of the degree of fragmentation. Hence the average intensity (over all returns of identical relative rank) was taken as an estimate of the contribution of a return to pulse interception. In other words, averaging out the high variability of target reflectivity, the mean relative intensity per return rank per number of returns, was expected to provide the best estimate of individual return contribution to laser pulse interception.

A more thorough examination of patterns of return intensity which was permitted by the comparison across sensors and settings revealed that loss of returned energy was not generally negligible.

It was found for two sensors that fragmentation reduced the cumulative retrieved energy (with losses of c. 10%-20% Figure 3A & B). The third sensor (VUX) which operated at the same wavelength as the sensor used in the 2017 study, showed no reduction in cumulative intensity with fragmentation, but rather the opposite pattern (Figure 3C and D). This pattern largely disappeared however once the dependency of return intensity on canopy depth was corrected for. The apparently stable cumulative return intensity observed probably reflected an imperfect correction of the dependency of individual return intensity on canopy depth which was based on single returns. Not only was the correction model applied fairly crude but also single returns further away from the top of the canopy were more likely to be incomplete (partially intercepted without detectable additional return) than returns occurring higher up in the canopy. This might have introduced a negative bias in the correction model.

The correction of this systematic variation in target reflectivity with canopy depth aimed at limiting the distortion between reflected energy and area of intercepting surface. However, it did not correct for detection bias.

The LMSQ780 2019 data which covered both ROIs showed a low level of dependence of intensity on canopy depth (Table 5) and a balanced ground to vegetation intensity (Table 7). We selected that dataset to develop a single statistical model of contribution of successive returns to laser pulse interception. Weights were first computed per ROI and were found to be very consistent across ROIs (Appendix 3). We then applied the same single matrix of individual return weights to all flights to compute light attenuation in AMAPVox.

Part 2 : intercalibration of extinction profiles

In this study we focused on two small ROIs (1.4 ha and 2 ha respectively) which did not capture the horizontal and vertical variability in vegetation structure found at the site level (10km^2). Detection bias is expected to vary with vegetation structure and show some variability both within and across sites (under constant acquisition settings). Previous work (Shao et al. 2019) suggests however that single intercalibration functions/coefficients may hold at site level, at least in first approximation.

Divergence of profiles (prior to intercalibration)

A systematic pattern of higher apparent extinction coefficient under lower at-canopy-irradiance (left most panel of Figure 4, Figure 5 and Figure 6) was found.

For a given system when the top of canopy irradiance increased (due to higher transmitted power, or lower flight height) the proportion of pulses reaching the ground (a measure of laser penetration) increased, i.e. ground detection rate increased (Table 1 & Table 2). Detection rate of the most distant targets was enhanced. While higher irradiance may, in principle, also improve detection of small close-by targets, the major impact was an increase in the detection of more distant targets.

The larger beam divergence of the miniVUX was responsible for a more rapid decrease in irradiance with increasing distance to laser. In addition, the received power is proportional to the inverse of the squared distance from laser to target (*Equation 2*). For a low flying altitude DLS, this distance varies by a factor of 2 and the power decreases by a factor 4 from top to bottom of canopy. Hence, detection rate by the miniVUX was expected to decrease significantly from top to bottom of canopy (Figure 4a). In fact, including this distance dependent correction proved critical for reducing residual standard error (Table 8) when flight height was lowest (and relative change in irradiance per unit distance was largest).

Effectiveness of intercalibration

Overall, calibration by a constant coefficient reduced the inter-profile residual standard error by a factor of ~2 while including distance to laser reduced the error by a factor of ~3 (Table 8 & Table 9). The level of initial discrepancy and the level of reduction in error was however highly variable across flights. The poorest fit (RMSE >0.01, ~relative RMSE >10%) occurred for VUX operated at low power (330kHz and 550kHz).

Source of residual misfit

The different detectability of ground, wood and leaves at 1550nm (Table 6**.** and (Brede et al. 2022)) was probably responsible for a complex distortion pattern of the profile at low power setting which prevented a simple model to effectively correct for this bias. At high power the level of under detection seemed to be limited though and a correction using distance to laser as covariate effectively aligned the VUX 100kHz profile to the reference ALS profile.

Absolute calibration

We selected the LMSQ780-25% power 2019 ALS flight covering both ROIs as the reference flight to which the attenuation profiles were fitted. However, comparison with lower altitude flights and higher at-canopy irradiance flights conducted with the same sensor on ROI1 (e.g. ALS_430m_12%) indicated that this attenuation reference profile was probably positively biased (by at least 16%, see Table 8). The same conclusion (likely positive attenuation bias) can be drawn from the comparison of the number of shots triggering a ground echo (7.3% for ALS_430m_12% - Table 2 - against 5.2% for ALS_900m_25% reference flight - Table 3).

A method for absolute calibration would be desirable as a reference flight will not usually be available across campaigns. This could be attempted by simulating light transfer in the voxelized scene and comparing light transmittance maps with measurement taken in situ (Vincent et al. 2017). However, given the high variation in time-integrated light intensity which is known to occur over short distances in the forest understory (Baraloto and Couteron 2010; Vincent et al. 2017), a dense ground sampling pattern would then be required, and any ground reference measurements would need to be accurately geo-positioned to be compared with the ALS data.

Another strategy would be to use terrestrial laser scanning to derive reference extinction coefficients for sample plots. Some terrestrial lasers have ranges in excess of 500m. Hence, they are unlikely to suffer from significant under-detection of vegetation below 50m range. There is however a difference in acquisition geometry due to sensors position. In TLS, the vegetation layers close to the ground are mostly sampled by pulses emitted at inclination angles close to the horizontal whereas the upper canopy layers are predominantly sampled with an angle close to the vertical. In case of strong anisotropy in light extinction, direct adjustment of attenuation profile derived with one sensor to the attenuation profile derived with the other may not yield valid results. In addition, absolute calibration of TLS derived attenuation rates would still be required noting that TLS systems also vary in wavelength, pulse duration and recording capabilities.

The most straightforward strategy would probably be to fly again over part of the scanned area at much higher at-canopy-irradiance, assuming that the under-detection bias would then be negligible. Comparing detection rate for gradually decreasing power may provide a way to check that detection rate reaches acceptable levels at maximum power. Modern lidar systems such as the LMSQ780 are designed for mapping large areas and are able to operate at high altitude (up to

4700m for the LMSQ780 according to the manufacturer's technical data sheet (RIEGL Laser Measurement Systems 2015). Flying at 900m (the cruising altitude of our reference flight) the at-canopy-irradiance could in principle be increased by a factor of 16 by increasing nominal power from 25% to 100% and decreasing PRR from 400KHz to 100KHz. At-canopy-irradiance could be increased further by flying lower if necessary. Hence there is a considerable margin to improve completeness of target detection without risking ocular hazard (Nominal Ocular Hazard Distance is given at 200m for the LMSQ780 lidar operated at full power 100kHz PRR) thereby achieving a robust estimate of the true detection bias affecting lidar data collected under standard settings.

Conclusion

We found that a more complete retrieval of backscattered energy was achieved in the case of higher at-canopy-irradiance. Incomplete target detection generated a positive bias in light attenuation coefficient and consequently in PAD. Positive bias was due to the fact that more distant targets were less consistently detected. In a series of hits along an optical path, foremost interceptions will tend to be larger as pulse effective footprint is larger. Therefore, foremost targets are more systematically detected. The general pattern can be modulated by differential reflectivity of ground and vegetation or of different vegetation elements.

Systematic increase of reflectivity with canopy depth observed at 1550nm had not been noted in a previous study conducted on the same site with another sensor operating at the same wavelength (Vincent et al. 2017). This variation in vegetation reflectivity probably masked a decrease in detection rate with fragmentation and led the authors to the wrong conclusion that detection bias was negligible.

Biases in light attenuation related to incomplete target detection may be large. Considering for instance the highest at-canopy irradiance experimented in the present study (ALS-430m 12% power) as the reference, it was observed that ALS attenuation profiles were typically overestimated by 15 to 20% and UAV by 20 to 25%. This means that PAD will also be overestimated in the same proportion. These are lower bound estimates of detection bias. True bias could be approached using as a reference a saturating at-canopy-irradiance (showing no increase in detection rate with further increase in at-canopy-irradiance).

Intercalibration of lidar overflights conducted with the LMSQ780 or miniVUX at different altitude or power settings was satisfactory. Sensors operating at wavelengths more different from each other were more difficult to intercalibrate and simple methods like those presented here were not totally effective. They notably failed to properly align low power VUX flights with the rest of the flights. A fine calibration between sensors operating at different wavelength would probably require reformulating the model which describes pulse interception by vegetation elements at voxel level by including an estimate of censorship. Predicting the likelihood of local under-detection may be possible but is not straightforward because target detectability will not only depend on effective footprint size and distance to laser as shown here, but also on unknown features such as optical properties, spatial arrangement and size of vegetation elements. TLS data which can give access to leaf-wood segmentation and, at least at close range, to the orientation of vegetation elements (Bailey and Mahaffee 2017; Vicari et al. 2019; Stovall et al. 2021) may provide an opportunity to integrate local correction for detection rate. However, transferability to landscape scale ALS data would remain an issue. The use of simulated data (Yin et al. 2020) may offer another avenue to model censorship based on the statistical analysis of the point cloud geometric and radiometric features.

Acknowledgements

This is a publication of Laboratoire d'Excellence CEBA (ANR-10-LABX-25). This study benefited from funding by the Centre National d’Etudes Spatiales [grant n°4500063412 and 4500066841 – Tosca BIOMASS], and the European Spatial Agency [ESA AO/1-9584/18/NL/AI FORESTSCAN]

Description of author's responsibilities.

Conceptualization, Writing - Original Draft GV; Methodology GV, PV, NB, BB; data collection NB, BB, GV, JB, IC; formal analysis GV, EM, GD; Software PV; Writing - Review & Editing ALL.

References

Almeida DRA de, Stark SC, Shao G, Schietti J, Nelson BW, Silva CA, Gorgens EB, Valbuena R, Papa D de A, Brancalion PHS (2019) Optimizing the Remote Detection of Tropical Rainforest Structure with Airborne Lidar: Leaf Area Profile Sensitivity to Pulse Density and Spatial Sampling. Remote Sensing 11:92. https://doi.org/10.3390/rs11010092

Arnqvist J, Freier J, Dellwik E (2020) Robust processing of airborne laser scans to plant area density profiles. Biogeosciences 17:5939–5952. https://doi.org/10.5194/bg-17-5939-2020

Bailey BN, Mahaffee WF (2017) Rapid measurement of the three-dimensional distribution of leaf orientation and the leaf angle probability density function using terrestrial LiDAR scanning. Remote Sensing of Environment 194:63–76. https://doi.org/10.1016/j.rse.2017.03.011

Baraloto C, Couteron P (2010) Fine-scale Microhabitat Heterogeneity in a French Guianan Forest. Biotropica 42:420–428. https://doi.org/10.1111/j.1744-7429.2009.00620.x

Bonan G (ed) (2015) Plant Canopies. In: Ecological Climatology: Concepts and Applications, 3rd edn. Cambridge University Press, Cambridge, pp 264–288

Bréda NJJ (2003) Ground-based measurements of leaf area index: a review of methods, instruments and current controversies. J Exp Bot 54:2403–2417

Brede B, Bartholomeus HM, Barbier N, Pimont F, Vincent G, Herold M (2022) Peering through the thicket: Effects of UAV LiDAR scanner settings and flight planning on canopy volume discovery. International Journal of Applied Earth Observation and Geoinformation 114:103056. https://doi.org/10.1016/j.jag.2022.103056

Chen JM, Black TA (1991) Measuring leaf area index of plant canopies with branch architecture. Agricultural and Forest Meteorology 57:1–12. https://doi.org/10.1016/0168-1923(91)90074-Z

Chen JM, Rich PM, Gower ST, Norman JM, Plummer S (1997) Leaf area index of boreal forests: Theory, techniques, and measurements. J Geophys Res 102:29429–29443. https://doi.org/10.1029/97JD01107

Fang H, Baret F, Plummer S, Schaepman-Strub G (2019) An Overview of Global Leaf Area Index (LAI): Methods, Products, Validation, and Applications. Reviews of Geophysics 57:739–799. https://doi.org/10.1029/2018RG000608

Frost C, Thompson SG (2000) Correcting for Regression Dilution Bias: Comparison of Methods for a Single Predictor Variable. Journal of the Royal Statistical Society Series A (Statistics in Society) 163:173–189

Höfle B, Pfeifer N (2007) Correction of laser scanning intensity data: Data and model-driven approaches. ISPRS Journal of Photogrammetry and Remote Sensing 62:415–433. https://doi.org/10.1016/j.isprsjprs.2007.05.008

Hopkinson C, Chasmer LE (2007) Modeling canopy gap fraction from lidar intensity. In: IAPRS Volume XXXVI. Espoo, Finland, p Part 3 / W52

Kaasalainen S, Hyyppa H, Kukko A, Litkey P, Ahokas E, Hyyppa J, Lehner H, Jaakkola A, Suomalainen J, Akujarvi A, Kaasalainen M, Pyysalo U (2009) Radiometric Calibration of LIDAR Intensity

With Commercially Available Reference Targets. IEEE Transactions on Geoscience and Remote Sensing 47:588–598. https://doi.org/10.1109/TGRS.2008.2003351

Laurans M, Martin O, Nicolini E, Vincent G (2012) Functional traits and their plasticity predict tropical trees regeneration niche even among species with intermediate light requirements. Journal of Ecology 100:1440–1452. https://doi.org/10.1111/j.1365-2745.2012.02007.x

Lee C-C, Wang C-K (2013) LiDAR Penetration Comparison at Different Altitudes and Scanning Angles in Subtropical Forest

Longo M, Saatchi S, Keller M, Bowman K, Ferraz A, Moorcroft PR, Morton DC, Bonal D, Brando P, Burban B, Derroire G, dos-Santos MN, Meyer V, Saleska S, Trumbore S, Vincent G (2020) Impacts of Degradation on Water, Energy, and Carbon Cycling of the Amazon Tropical Forests. Journal of Geophysical Research: Biogeosciences n/a:e2020JG005677. https://doi.org/10.1029/2020JG005677

Miller J (1967) A formula for average foliage density. Australian Journal of Botany 15:141–144. https://doi.org/10.1071/BT9670141

Morsdorf F, Kötz B, Meier E, Itten KI, Allgöwer B (2006) Estimation of LAI and fractional cover from small footprint airborne laser scanning data based on gap fraction. Remote Sensing of Environment 104:50–61

Næsset E (2009) Effects of different sensors, flying altitudes, and pulse repetition frequencies on forest canopy metrics and biophysical stand properties derived from small-footprint airborne laser data. Remote Sensing of Environment 113:148–159. https://doi.org/10.1016/j.rse.2008.09.001

Olivas PC, Oberbauer SF, Clark DB, Clark DA, Ryan MG, O'Brien JJ, Ordoñez H (2013) Comparison of direct and indirect methods for assessing leaf area index across a tropical rain forest landscape. Agricultural and Forest Meteorology 177:110–116. https://doi.org/10.1016/j.agrformet.2013.04.010

Osada N, Takeda H, Furukawa A, Awang M (2001) Leaf dynamics and maintenance of tree crowns in a Malaysian rain forest stand. Journal of Ecology 89:774–782

R Core Team. (2022) R: A language and environment for statistical computing

Reich PB, Uhl C, Walters MB, Prugh L, Ellsworth DS (2004) Leaf demography and phenology in Amazonian rain forest: A census of 40 000 leaves of 23 tree species. Ecological Monographs 74:3–23

Riegl Laser Measurement Systems (2019) LAS extrabytes implementation in RIEGL software - WHITEPAPER. Riegl Laser Measurement Systems GmbH

RIEGL Laser Measurement Systems (2020) RIEGL VUX-1UAV Datasheet

RIEGL Laser Measurement Systems (2015) RIEGL LMS-Q780 Datasheet

RIEGL Laser Measurement Systems (2022) RiParameter

Ross J (1981) The radiation regime and architecture of plant stands. Springer Netherlands

Shabanov NV, Huang D, Yang W, Tan B, Knyazikhin Y, Myneni RB, Ahl DE, Gower ST, Huete AR, Aragao LEOC, Shimabukuro YE (2005) Analysis and optimization of the MODIS leaf area index algorithm retrievals over broadleaf forests. IEEE Transactions on Geoscience and Remote Sensing 43:1855–1865. https://doi.org/10.1109/TGRS.2005.852477

Shao G, Stark SC, de Almeida DRA, Smith MN (2019) Towards high throughput assessment of canopy dynamics: The estimation of leaf area structure in Amazonian forests with multitemporal multi-sensor airborne lidar. Remote Sensing of Environment 221:1–13. https://doi.org/10.1016/j.rse.2018.10.035

Solberg S, Brunner A, Hanssen KH, Lange H, Næsset E, Rautiainen M, Stenberg P (2009) Mapping LAI in a Norway spruce forest using airborne laser scanning. Remote Sensing of Environment 113:2317–2327. https://doi.org/10.1016/j.rse.2009.06.010

Stovall AEL, Masters B, Fatoyinbo L, Yang X (2021) TLSLeAF: automatic leaf angle estimates from single-scan terrestrial laser scanning. New Phytologist 232:1876–1892. https://doi.org/10.1111/nph.17548

Vicari MB, Pisek J, Disney M (2019) New estimates of leaf angle distribution from terrestrial LiDAR: Comparison with measured and modelled estimates from nine broadleaf tree species. Agricultural and Forest Meteorology 264:322–333. https://doi.org/10.1016/j.agrformet.2018.10.021

Vincent G, Antin C, Laurans M, Heurtebize J, Durrieu S, Lavalley C, Dauzat J (2017) Mapping plant area index of tropical evergreen forest by airborne laser scanning. A cross-validation study using LAI2200 optical sensor. Remote Sensing of Environment 198:254–266. https://doi.org/10.1016/j.rse.2017.05.034

Vincent G, Pimont F, Verley P (2021) A note on PAD/LAD estimators implemented in AMAPVox 1.8

Vincent G, Sabatier D, Blanc L, Chave J, Weissenbacher E, Pélissier R, Fonty E, Molino JF, Couteron P (2012) Accuracy of small footprint airborne LiDAR in its predictions of tropical moist forest stand structure. Remote Sensing of Environment 125:23–33. https://doi.org/10.1016/j.rse.2012.06.019

Vincent G, Weissenbacher E, Sabatier D, Blanc L, Proisy C, Couteron P (2010) Détection des variations de structure de peuplements en forêt dense tropicale humide par Lidar aéroporté (Small foot-print airborn LiDAR proves highly sensitive to changes in structure of moist tropical forest). Revue Française de Photogrammétrie et Télédétection 191:42–50

Wagner W (2010) Radiometric calibration of small-footprint full-waveform airborne laser scanner measurements: Basic physical concepts. ISPRS Journal of Photogrammetry and Remote Sensing 65:505–513. https://doi.org/10.1016/j.isprsjprs.2010.06.007

WeiChen H, Shih TianYuan [Shih TYP, HungCheng C, JinKing L (2015) A study on factors affecting airborne LiDAR penetration. TAO - Terrestrial, Atmospheric and Oceanic Sciences 26:241–251

Wojtanowski J, Zygmunt M, Kaszczuk M, Mierczyk Z, Muzal M (2014) Comparison of 905 nm and 1550 nm semiconductor laser rangefinders' performance deterioration due to adverse environmental conditions. Opto-Electron Rev 22:183–190. https://doi.org/10.2478/s11772-014-0190-2

Yin T, Qi J, Cook BD, Morton DC, Wei S, Gastellu-Etchegorry J-P (2020) Modeling Small-Footprint Airborne Lidar-Derived Estimates of Gap Probability and Leaf Area Index. Remote Sensing 12:4. https://doi.org/10.3390/rs12010004

Zheng G, Moskal LM (2009) Retrieving Leaf Area Index (LAI) Using Remote Sensing: Theories, Methods and Sensors. Sensors 9:2719–2745. https://doi.org/10.3390/s90402719